THE ASTROPHYSICAL JOURNAL, 492:L139–L142, 1998 January 10

SPATIALLY RESOLVED STIS SPECTROSCOPY OF SN 1987A: EVIDENCE FOR SHOCK INTERACTION WITH CIRCUMSTELLAR GAS[1]

G. SONNEBORN,[2] C. S. J. PUN,[2,3] R. A. KIMBLE,[2,4] T. R. GULL,[2,4] P. LUNDQVIST,[5] R. MCCRAY,[6] P. PLAIT,[7] A. BOGGESS,[4,8] C. W. BOWERS,[2,4] A. C. DANKS,[4,9] J. GRADY,[10] S. R. HEAP,[2,4] S. KRAEMER,[4,11] D. LINDLER,[7] J. LOIACONO,[10] S. P. MARAN,[4,12] H. W. MOOS,[4,13] AND B. E. WOODGATE[2,4]

Received 1997 August 6; accepted 1997 October 30; published 1997 December 30

ABSTRACT

Visual and ultraviolet spatially resolved (~0″.1) spectra of SN 1987A obtained on days 3715 and 3743 with the Space Telescope Imaging Spectrograph on the *Hubble Space Telescope* show that the high-velocity supernova debris is colliding with circumstellar gas. Very broad Lyα emission with velocities extending to $\sim \pm 20{,}000$ km s^{-1} originates *inside* the inner circumstellar ring and appears to fill most of the surface area within 0″.67 ± 0″.03 (0.14 pc at a distance of 50 kpc) of the ring's center. The observed Lyα flux from the shocked ejecta is $(1.85 \pm 0.53) \times 10^{-13}$ and $(1.25 \pm 0.51) \times 10^{-12}$ ergs cm^{-2} s^{-1} after correcting for extinction. A spatially *unresolved* blueshifted emission feature was discovered in Hα (and other lines) on the inner ring at position angle 31° ± 8°. The Hα emission extends to −250 km s^{-1} with no corresponding redshifted emission. This highly localized interaction appears to be the initial contact of the supernova blast wave with an inward protrusion of the inner ring. The broad Lyα emission and the "hot spot" are separate interaction phenomena associated with the reverse and forward shocks, respectively. We also find that the size of the inner ring in forbidden lines of oxygen has a dependence on ionization potential, in agreement with photoionization models of the ring.

Subject heading: circumstellar matter — supernova remnants — supernovae: individual (SN 1987A)

1. INTRODUCTION

SN 1987A in the Large Magellanic Cloud (LMC) continues to provide new opportunities to study the late-time evolution of supernovae and to probe their stellar origins. The collision of the ejecta with the progenitor's circumstellar (CS) medium has been anticipated since its discovery in mid-1987, due to its proximity to the supernova (Fransson et al. 1989). The coincident emergence of radio (Staveley-Smith et al. 1992, 1993) and X-ray (Beuermann, Brandt, & Pietsch 1994) emission in 1990, their subsequent monotonic increase, and the deceleration of the supernova shock (Staveley-Smith et al. 1993) indicate that the high-velocity supernova (SN) shock encountered low-density CS gas starting around 1200 days after the explosion. This gas corresponds to mass lost by the progenitor near the end of its red supergiant (RSG) phase (Chevalier & Dwarkadas 1995, hereafter CD95). Gaensler et al. (1997) find that the radio-emitting region is located just inside the central ring, based on a ~0″.4 resolution 9 GHz map, and is expanding at ~2800 km s^{-1} (12 mas yr^{-1}). The shock interaction region, bounded by forward and reverse shocks, consists of an outer zone of shocked CS gas and an inner zone of shocked ejecta (Chevalier 1982).

The SN 1987A CS medium is a fossil record of the pre-explosion mass loss and may hold important clues to the nature of the progenitor (e.g., single vs. binary star). The gas in the central ring ($n_e \sim 10^4$ cm^{-3}) is significantly enhanced in helium and nitrogen, indicating that the progenitor was in a post–He-core burning phase when it exploded (Fransson et al. 1989; Sonneborn et al. 1997). The presence of lower density gas ($n_e \sim 100$ cm^{-3}; CD95) inside the ring traces the mass loss at the end of the RSG stage, after formation of the inner ring.

The small angular extent and complex structure of the SN 1987A CS gas and debris require the high spatial resolution of the *Hubble Space Telescope* (*HST*). The Wide Field Planetary Camera 2 (WFPC2) and Faint Object Camera (FOC) imagery revealed the remarkable thin-ring structures (Jakobsen et al. 1991, [O III]; Burrows et al. 1995, Hα; Plait et al. 1995, [N II]). However, the first-generation *HST* spectrographs had one-dimensional detectors and could only provide spatial information on the scale of the available apertures. The Space Telescope Imaging Spectrograph (STIS) provides imaging spectroscopy by combining the excellent optical performance of imaging optics with two-dimensional detectors (Kimble et al. 1998). With good spectral resolution and *HST*-limited spatial resolution, we are now able to study the spatial dependence of the line emission from the inner ring and do the first spectral analysis of the interaction of the SN ejecta with the CS gas. In an accompanying Letter, Michael et al. (1998, hereafter M98)

[1] Based on observations with the NASA/ESA *Hubble Space Telescope*, obtained at the Space Telescope Science Institute, which is operated by the Association of Universities for Research in Astronomy, Inc., under NASA contract NAS5-26555.

[2] Laboratory for Astronomy and Solar Physics, Code 681, NASA Goddard Space Flight Center, Greenbelt, MD 20771; sonneborn@stars.gsfc.nasa.gov, kimble@stars.gsfc.nasa.gov, gull@stars.gsfc.nasa.gov, bowers@stars.gsfc.nasa.gov, hrsheap@stars.gsfc.nasa.gov, woodgate@stars.gsfc.nasa.gov.

[3] National Optical Astronomy Observatories, P.O. Box 26732, 950 North Cherry Avenue, Tucson, AZ 85726-6732; pun@congee.gsfc.nasa.gov.

[4] Space Telescope Imaging Spectrograph Investigation Definition Team.

[5] Stockholm Observatory, S-13336, Saltsjöbaden, Sweden; peter@astro.su.se.

[6] JILA, Campus Box 440, University of Colorado, Boulder, CO 80309; dick@jila.colorado.edu.

[7] Applied Computer Concepts, Code 681, NASA Goddard Space Flight Center, Greenbelt, MD 20771; plait@abba.gsfc.nasa.gov, lindler@rockit.gsfc.nasa.gov.

[8] 2420 Balsam Drive, Boulder, CO 80304; boggess@lyrae.colorado.edu.

[9] Hughes STX, Code 681, NASA Goddard Space Flight Center, Greenbelt, MD 20771; danks@stars.gsfc.nasa.gov.

[10] Laboratory for Astronomy and Solar Physics, Code 680.1, NASA Goddard Space Flight Center, Greenbelt, MD 20771; grady@stars.gsfc.nasa.gov, loiacono@stars.gsfc.nasa.gov.

[11] Catholic University of America, Code 681, NASA Goddard Space Flight Center, Greenbelt, MD 20771; kraemer@stars.gsfc.nasa.gov.

[12] Space Sciences Directorate, Code 600, NASA Goddard Space Flight Center, Greenbelt, MD 20771; hrsmaran@eclair.gsfc.nasa.gov.

[13] Department of Physics and Astronomy, Johns Hopkins University, Baltimore, MD 21218; hwm@pha.jhu.edu.

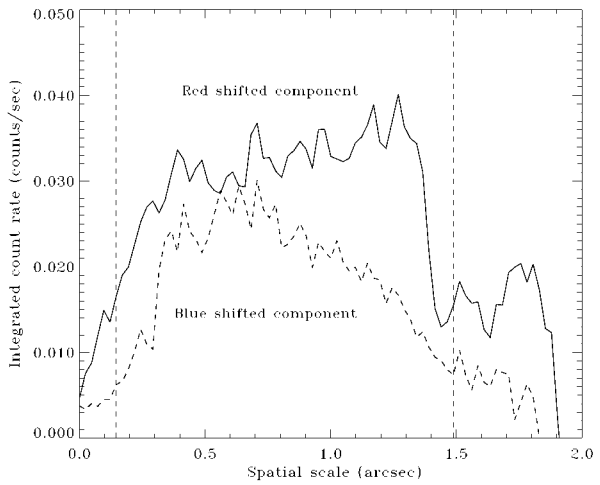

FIG. 4.—Spatial distribution of the Lyα emission along the aperture. The spatial scale goes from the lower edge (0″) to the top edge (2″). The crosscut in the red wing was made at 1250 ± 8 Å, and at 1179 ± 8 Å in the blue wing. The vertical dashed lines mark the location of the inner edge of the CS ring.

model the CS interaction and the emission processes that produce the Lyα emission discussed below.

2. OBSERVATIONS

2.1. *Ultraviolet Spectral Imaging*

Ultraviolet spectral images of SN 1987A and the inner CS ring were taken with the STIS far-ultraviolet (FUV) MAMA detector on 1997 May 24 (3743 days after core collapse). Two exposures (Pgm ID 7123) were taken in time-tag mode with the G140L grating (~1130–1720 Å) for a total exposure time of 4180 s. The plate scale of the image is 0.″0244 pixel^{-1} in both the spatial and spectral directions. The spatial resolution is ~0.″06. The G140L spectral resolution is ~1.2 Å (0.5833 Å pixel^{-1}). The 2″ × 2″ aperture was chosen to include the entire inner circumstellar ring (1.″7 × 1.″2; Plait et al. 1995) and exclude the neighboring B stars, primarily star 3 ($V \sim 16$, 1.″6 from the SN; see Fig. 1*a* [Pl. L31]). The G140L spectral image is shown in Figure 2 (Plate L32).

A striking and previously unobserved emission feature, extending from $\lesssim$1145 to ~1300 Å, is identified as Lyα from the shock interaction of the high-velocity debris with CS gas. The strong radiation filling the square aperture is geocoronal Lyα. The diffuse continuum extending the length of the spectrum is UV background from the LMC. The detector background count rate is extremely low ($<1 \times 10^{-5}$ counts s^{-1} pixel^{-1}; Kimble et al. 1998) and is negligible in the data. Images of the inner ring are also detected in O IV] λλ1397–1407, N IV] λ1486.5, and He II λ1640.5; their orientation indicates that the aperture's spatial axis is at a position angle (p.a.) of 115° ± 4°. A weak, spatially extended UV continuum (1400–1700 Å) from the debris is also present.

Wavelength calibration exposures using the Pt-Cr/Ne line lamp were taken through the 52″ × 0.″1 slit for each G140L exposure. The absolute wavelength scale was referenced to the small offset (Δx) of the SN from the center of the aperture. We find the SN offset to be $\Delta x = +0.''12 \pm 0.''15$ in the dispersion direction and $\Delta y = -0.''17 \pm 0.''04$ in the spatial direction, as determined from the center of the ring in O IV], N IV], and He II.

2.2. *Visible Spectral Imaging*

Medium-resolution spectral images (Pgm ID 7123) of the inner ring were obtained in two grating settings on 1997 April 26 (day 3715): G750M (6295–6867 Å, resolution = 1.02 Å, 643 s), and G430M (4818–5104 Å, resolution = 0.83 Å, 828 s). The 52″ × 2″ slit was chosen to include the entire ring and was oriented along its major axis (Fig. 1*b*), thereby providing maximum separation in the dispersion direction between images of the ring in adjacent emission lines. The narrow emission lines from the ring ($v_{\rm FWHM} \lesssim 15$ km s^{-1}) remain spectrally unresolved in these observing modes ($\Delta v \sim 50$ km s^{-1}), while the debris spectral features ($v_{\rm FWHM} \sim 2500$ km s^{-1}) are highly dispersed. In addition to the CS ring and the SN debris, the G750M and G430M spectral images (see Fig. 3 [Pl. L33]) also show diffuse Hα, Hβ, and [O III] emission filling the long slit and the continuous spectra of star 3 (including stellar Hα and Hβ emission lines) and several fainter stars.

An [O II] λ3727 image (Pgm ID 7122) of SN 1987A and its ring system was taken with STIS on 1997 April 4 (day 3693), using the F28X50OII filter. Four exposures totaling 2415 s were obtained.

3. RESULTS

3.1. *Ultraviolet Spectroscopy*

The Lyα emission from SN 1987A reported here is the signature of the shock interaction between high-velocity SN ejecta and CS gas inside the bright inner ring. Two aspects of the Lyα feature are particularly noteworthy: (1) the spatial and velocity distribution of the Lyα flux, and (2) the relative brightnesses of the red and blue wings of the line profile.

We measure the red edge of the Lyα profile at 1301.7 ± 3.7 Å, or 20,900 ± 900 km s^{-1} relative to 1216.825 Å (Lyα in the LMC rest frame). However, the red edge could be as large as 1328 Å (27,400 km s^{-1}), depending on the details of the diffuse background subtraction. A Doppler shift of −20,900 km s^{-1} on the blue side of the profile occurs at 1131 Å. Unfortunately, we cannot measure the profile shortward of ~1145 Å because of decreasing *HST*/STIS sensitivity below 1170 Å. Measurement of the blue wing of the Lyα profile awaits observations by the *Far-Ultraviolet Spectroscopic Explorer* in 1999.

The Lyα brightness profile in the spatial direction (across the spectrum) sets a limit on the spatial extent of the shock interaction region in a direction close to the major axis of the ring. Figure 4 shows spatial brightness profiles in the blue and red wings of Lyα. The Lyα surface brightness is fairly uniform, and there is no significant brightening along the upper and lower edges of the feature (cf. M98). The spatial extent is 1.″22 ± 0.″06 and 1.″14 ± 0.″11 on the red (1250 ± 8 Å) and blue (1179 ± 8 Å) sides of the aperture. The projected size of the ring in the observing geometry is 1.″51 ± 0.″06, based on the ring size in [O III] (Plait et al. 1995). Thus, the interaction region is located at 79% ± 4% of the ring's radius, or $\sim 5 \times 10^{17}$ cm from the center of the debris. The spatial extent of the interaction region in the dispersion direction cannot be measured directly from the STIS data, owing to the fact that the observed (x, y) distribution of Lyα photons is a convolution of the geometry and the velocity field. The separation of the two effects is model dependent (M98), but the spatial extent is probably $\lesssim$1.″4. The blue and red wings are tapered toward higher velocities, and the maximum Doppler shift is roughly aligned with the center of the ring.

The Lyα line profile (Fig. 5) is the sum of the observed count rate at each wavelength point multiplied by the G140L sensitivity function. The integrated observed flux assumes that the part of the Lyα profile obscured by geocoronal emission decreases linearly from 1187.0 to 1241.3 Å (see Fig. 5), corresponding to the edges of the 2″ wide aperture in the G140L image. The points where the profile meets the background are 1144.4 and 1301.7 Å. The integrated Lyα flux is $(1.85 \pm 0.53) \times 10^{-13}$ ergs cm^{-2} s^{-1}, consistent with the hydrodynamical models of Borkowski, Blondin, & McCray (1997). The dereddened Lyα flux is $(1.25 \pm 0.51) \times 10^{-12}$ ergs cm^{-2} s^{-1} [$E(B - V) = 0.16$; Fitzpatrick & Walborn 1990]. The dereddened fluxes from the observable portions of the profile are $(3.3 \pm 0.9) \times 10^{-13}$ ergs cm^{-2} s^{-1} (1144.4–1187.0 Å) and $(2.3 \pm 0.5) \times 10^{-13}$ ergs cm^{-2} s^{-1} (1241.3–1301.7 Å). This asymmetry is probably due to the ~10 month light-travel time across the interaction region, implying a short timescale for changes in the shock spectrum. Dust in the ejecta might also be a factor. There is no conclusive evidence for N v λ1240 emission from the shocked gas (see M98). The intensity variations in the red wing may be the result of strong interstellar absorption lines (e.g., 1260, 1300, and 1335 Å; cf. Sonneborn et al. 1997) convolved with the spatial extent of the interaction region.

There are significant uncertainties in the Lyα flux measurements. The net effect of statistical errors is very small (<1%) and is negligible by comparison with the other error sources: the geometry of the interaction region, the systematic errors in the flux measurement, interstellar extinction, and the *HST*/STIS G140L sensitivity function.

We estimate that the uncertainty in the evaluation of the Lyα flux hidden by geocoronal emission (see Fig. 5) is ~25%. The estimated uncertainty in the preliminary G140L sensitivity function used for this flux calculation is ~10% longward of ~1240 Å and increases to ~20% at the shortest wavelengths. (The postlaunch STIS calibration is currently underway, and the expected uncertainty for the complete sensitivity function should be $\lesssim$5% for all wavelengths.) Other potential sources of systematic error include the selection of the endpoints of the integration regions and background subtraction.

The spatial extent of the CS interaction region in the dispersion direction ($\pm 0\farcs7 = \pm 16.7$ Å $= \pm 4100$ km s^{-1}) introduces uncertainties in the calibrated Lyα profile, unless its geometry is known and modeled. If the Lyα surface brightness is symmetric, as may be the case for SN 1987A (M98), this effect would be reduced significantly. Nevertheless, we estimate this uncertainty to be 20%–25% of the Lyα flux.

Errors in the Galactic and LMC extinction laws, in particular at $\lambda < 1200$ Å, are an additional source of error in the dereddened flux. The uncertainty in the extinction law near 1200 Å is about 10% (Fitzpatrick & Walborn 1990), while for 1140–1200 Å we estimate it to be ~20%. The uncertainty in $E(B - V)$ for SN 1987A is 0.02 mag (Fitzpatrick & Walborn 1990). The net uncertainty due to extinction is ~25%. Combining these error sources, the total estimated uncertainty in the observed Lyα flux is 30%–35% (38%–43% for the dereddened flux).

Apart from the Lyα emission, the inner ring is detected in the G140L image in O IV] λλ1397–1407, N IV] λ1486.5, and He II λ1640.5 (see Fig. 2), indicating that a significant fraction of hot gas remains in the ring. The dereddened surface brightnesses for O IV], N IV], and He II are (6.0 ± 1.4), (10.8 ± 2.3), and $(15.4 \pm 3.4) \times 10^{-15}$ ergs cm^{-2} s^{-1} arcsec^{-2}, respectively. In addition, a faint and spatially extended far-UV continuum of the SN debris (FWZI ~ 0″.44 and centered on the O IV], N IV], and He II images of the ring) is detected longward of 1400 Å with an average dereddened flux of $(1.6 \pm 0.6) \times 10^{-16}$ ergs cm^{-2} s^{-1} Å^{-1}. Although a $V \sim 20$ A5 star (Plait et al. 1995) is superposed on the ring at p.a. = 227° (see Fig. 1), such a star would contribute less than 5% of the observed flux. There is no evidence for a point-source spectrum in the G140L data.

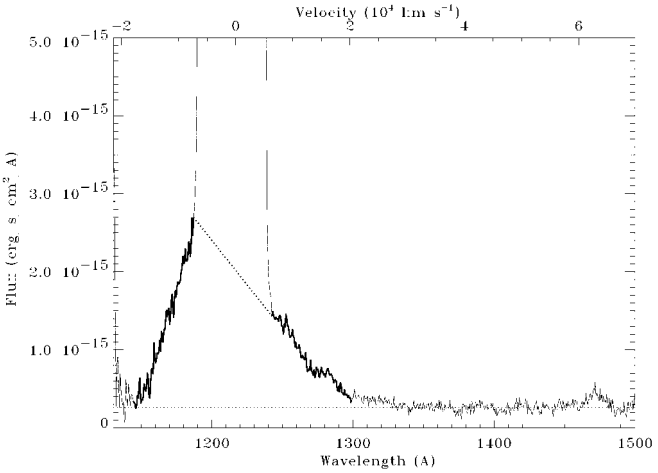

FIG. 5.—Calibrated STIS G140L spectrum of SN 1987A. The thick solid line indicates where the Lyα profile was measured for the integrated flux. The CS Lyα emission within the aperture is approximated by the broken line. The feature at 1470 Å is a combination of N IV] and SN debris.

3.2. *Visible Spectroscopy*

The STIS G430M and G750M observations of SN 1987A yield nearly monochromatic images of the inner CS ring in a large number of lines: Hβ, [O III] λλ4958.9, 5006.8, [O I] λλ6300.3, 6363.8, [N II] λλ6548.0, 6583.4, Hα, and [S II] λλ6716.5, 6730.8 are observed. Parts of the outer rings are noticeable in Hα, [N II], and [O III]. Hα emission from the SN debris is detected as a very broad, spatially resolved emission feature passing through the center of the [N II] and Hα ring images. The observed images of the ring (Fig. 6 [Pl. L34]) have similar morphology and intensity variations.

These spectral images revealed a spatially *unresolved*, and previously unknown, blueshifted Hα emission feature (also detected in Hβ, [O I] λ6300, and [O III] λ5007) located close to or on the inner ring at p.a. = $31° \pm 8°$ (Pun et al. 1997). The Hα emission extends to -250 km s^{-1} with no corresponding redshifted emission (see Fig. 6*d*). Garnavich, Kirshner, & Challis (1997) pinpointed this "hot spot" when they found a brightening at the same p.a., but located slightly inside the ring, in 1997 July WFPC2 Hα, [O III], and broadband images. The hot spot must be a separate phenomenon from that producing the spatially extended, high-velocity Lyα emission. It may be a manifestation of the initial encounter of the SN blast wave with an inward protrusion of the inner ring. If so, we would expect it to continue to brighten rapidly, and that more such spots will appear during the next few years.

The STIS observations also help determine the location of the outer rings relative to the SN. A portion of the northern outer ring is projected on the SN debris (cf. Fig. 1). In Figure 6*d*, the image of this ring in [N II] λ6583 has a ~0″.3 gap where it crosses the SN position, indicating that this section is located behind the debris.

The size of the ring as a function of p.a. in [O I] λ6300, [O II] λ3727, [O III] λ5007, and [S II] λ6731 is shown in Figure 7. In most places, the ring size in the oxygen lines increases with the ionization stage. The radius is most reliably measured at the *E* ansa (p.a. = 88°), where $\theta = 0\farcs792$ and $0\farcs845$ for [O I] and [O III], respectively. The [S II] λ6716/λ6731 and [N II] λ6548/λ6583 line ratios (Fig. 8 [Pl. L35]) are more uniform than the individual line images (Fig. 6). The mean [S II] ratio is 0.54 ± 0.02, corresponding to $N_e = 6000$ cm^{-3}. This is similar to that found by Lundqvist et al. (1998), based on an analysis of *HST*/Faint Object Spectrograph ring spectra from earlier epochs at p.a. ~ 300°. The presence of a significant ionization gradient in the ring and a fairly uniform density for the emitting gas are consistent with the photoionization/recombination models (Lundqvist & Fransson 1996; Lundqvist & Sonneborn 1997).

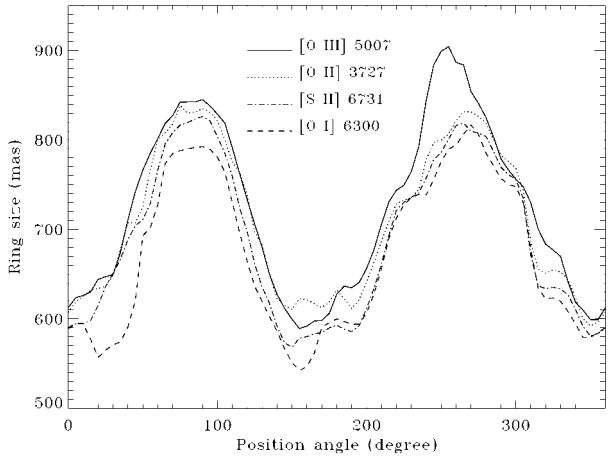

FIG. 7.—Size of the SN 1987A inner CS ring as a function of position angle in the light of several emission lines.

4. CONCLUSIONS

STIS UV spectral imaging has further characterized the shock interaction region around SN 1987A. Broad Lyα emission originates *inside* the inner ring, at ~80% of the ring's radius, corresponding to the location of the reverse shock front (M98). The fairly uniform Lyα surface brightness and large Doppler shifts indicate that the shock geometry is not confined to the plane of the inner ring and may in fact be spheroidal, as shown by M98. This may provide evidence about the geometry of the RSG wind above and below the ring plane. The emerging picture of the debris-CS gas interaction region is close indeed to that proposed by CD95. The asymmetry between the blue and red wings of Lyα indicates that the emission from the reverse shock may be evolving on a timescale of months. The location of the reverse shock is consistent with unimpeded debris expansion at ~40,000 km s^{-1} up to ~1200 days, when the radio emission picked up, followed by expansion of the shock at ~2800 km s^{-1} to the present.

The hot spot discovered at p.a. = 31° appears to be a different, highly localized shock interaction phenomenon closer to the ring than that observed in Lyα. The location of the hot spot indicates that the forward shock has reached the innermost edge, or an inward protrusion, of dense ring material. This places the forward shock at ~1.1 times the reverse shock radius. If this picture is correct, similar hot spots may light up around the ring in the coming years, providing a detailed map of the ring's radial geometry.

We are grateful to Bob Kirshner and the SINS collaboration for sharing their recent WFPC2 results with us before publication, and to Roger Chevalier and Claes Fransson for useful discussions. We thank the staff of the Space Telescope Science Institute and the STIS Team at GSFC and Ball Aerospace for their support, and the *HST* Project for the opportunity to make these observations as part of the Early Release Observation program.

REFERENCES

Beuermann, K., Brandt, S., & Pietsch, W. 1994, A&A, 281, L45
Borkowski, K., Blondin, J., & McCray, R. 1997, ApJ, 476, L31
Burrows, C. J., et al. 1995, ApJ, 454, 680
Chevalier, R. A. 1982, ApJ, 258, 790
Chevalier, R. A., & Dwarkadas, V. V. 1995, ApJ, 452, L45 (CD95)
Fitzpatrick, E. F., & Walborn, N. R. 1990, AJ, 99, 1483
Fransson, C., et al. 1989, ApJ, 336, 429
Gaensler, B. M., Manchester, R. N., Staveley-Smith, L.,Tzioumis, A. K., Reynolds, J. E., & Kesteven, M. J. 1997, ApJ, 479, 845
Garnavich, P., Kirshner, R. P., & Challis, P. 1997, IAU Circ. 6710
Jakobsen, P., et al. 1991, ApJ, 369, L63
Kimble, R. A., et al. 1998, ApJ, 492, L83
Lundqvist, P., et al. 1998, in preparation
Lundqvist, P., & Fransson, C. 1996, ApJ, 464, 924
Lundqvist, P., & Sonneborn, G. 1997, in SN 1987A: Ten Years After, the Fifth CTIO/LCO Workshop, ed. N. B. Suntzeff & M. M. Phillips (San Francisco: ASP), in press
Michael, E., McCray, R., Borkowski, K. J., Pun, C. S. J., & Sonneborn, G. 1998, ApJ, 492, L143 (M98)
Plait, P., et al. 1995, ApJ, 439, 730
Pun, C. S. J., et al. 1997, IAU Circ. 6665
Sonneborn, G., et al. 1997, ApJ, 477, 848
Staveley-Smith, L., et al. 1992, Nature, 355, 147
———. 1993, Nature, 366, 136

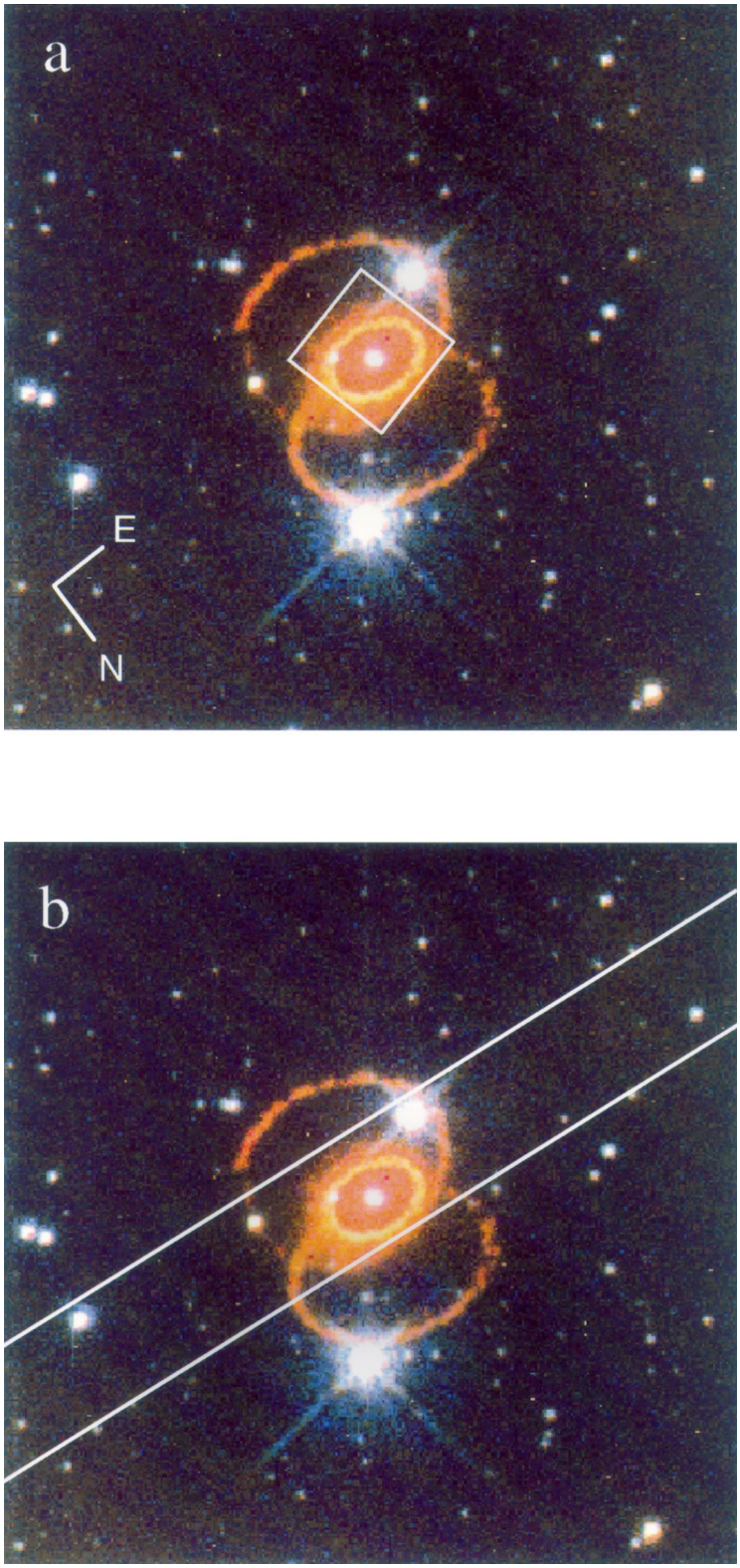

FIG. 1.—The size and location of the STIS apertures are shown on a 1995 composite WFPC2 image of SN 1987A (courtesy of P. Challis, R. Kirshner, and the SINS collaboration). The image size is 13″ square. (*a*) The 2″ × 2″ aperture location for the G140L observation. (*b*) The 52″ × 2″ aperture orientation (p.a. = 87°) for the G430M and G750M exposures.

SONNEBORN et al. (see 492, L140)

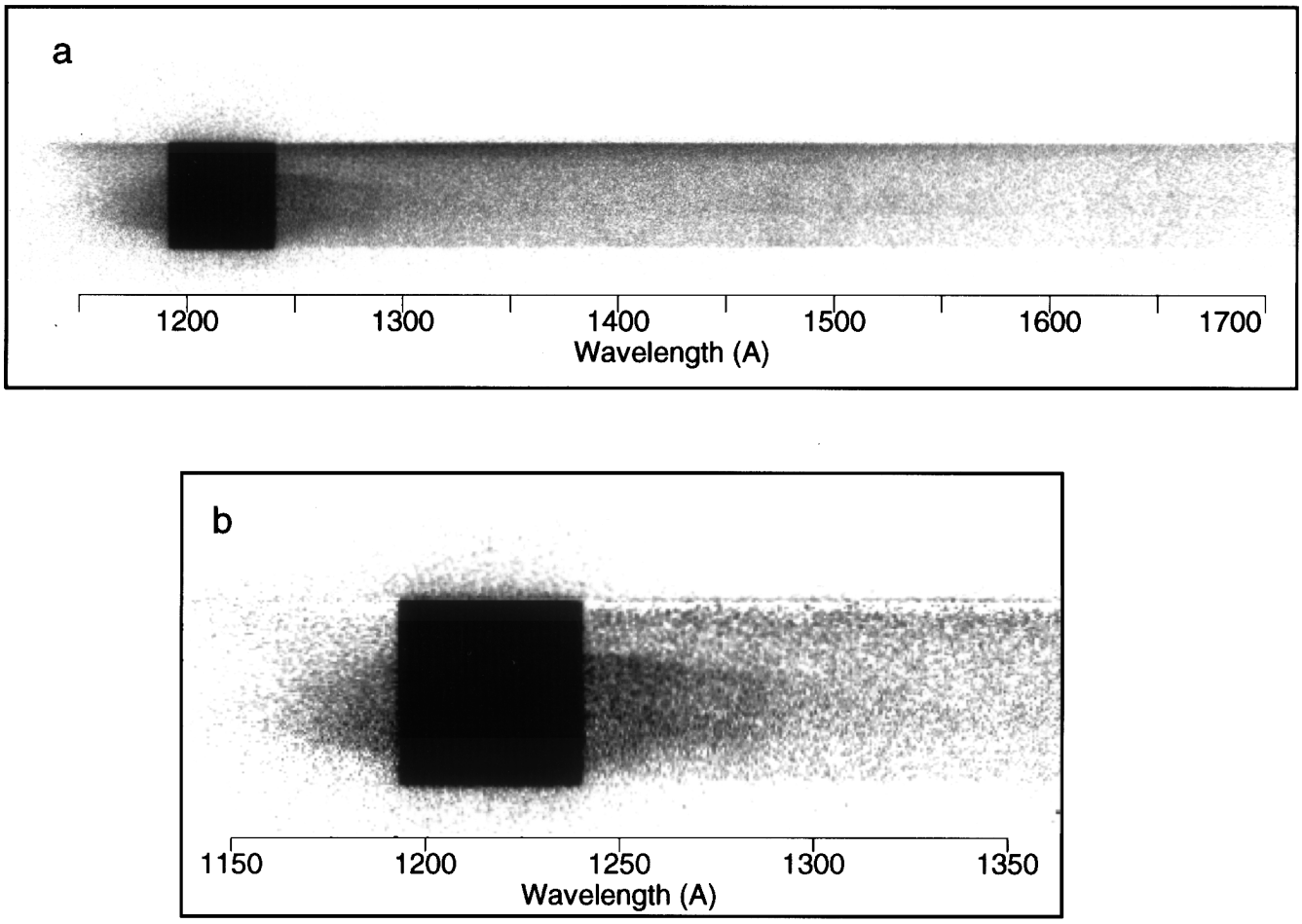

FIG. 2.—(*a*) STIS FUV MAMA G140L (1130–1720 Å) raw spectral image of SN 1987A. The image was reconstructed from time-tag mode data. The displayed image is a 1024 × 300 pixel subarray of the 1024 × 1024 image. Although star 3 lies outside the aperture, some light from it is still detected in the G140L image as the continuum emission along the top edge of the spectrum. (*b*) Expanded view of (*a*), with background corrections. The flux from star 3 was subtracted with row-by-row continuum fits to the data. The diffuse background was approximated by extracting the spectrum in the ~0.″2 gap between the extended Lyα emission and the light from star 3. This spectrum was subtracted from every row of the image after it was scaled to match the gradient in the background along the slit. Both images are displayed on a logarithmic intensity scale. Wavelength scales are shown in the LMC rest frame.

SONNEBORN et al. (see 492, L140)

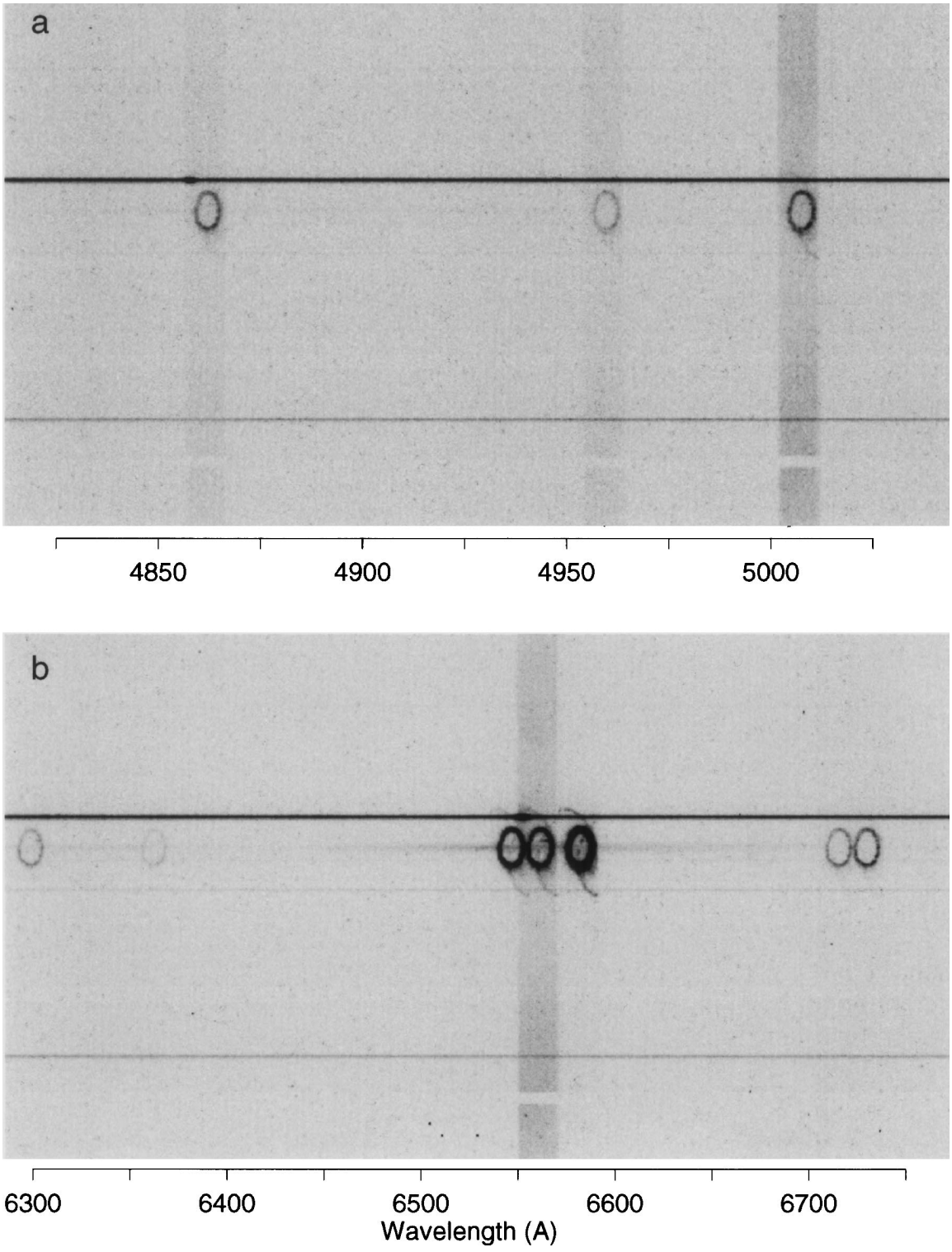

FIG. 3.—(*a*) The STIS G430M 4851 Å spectral image of SN 1987A shows the images of the inner CS ring in Hβ and [O III] λ4959 and λ5007. These lines are also present in diffuse emission from the LMC filling the $52'' \times 2''$ aperture. The bright point-source spectrum is from star 3. The image shown is a 950 × 450 pixel subarray of the 1024 × 1024 image. The image was processed to remove cosmic rays and hot pixels. (*b*) Same as (*a*), but for the G750M 6581 Å exposure. The images are shown on a logarithmic intensity scale, and the contrast is stretched to enhance weaker features. The spatial scales in the dispersion and cross-dispersion directions are not identical in the raw G430M and G750M images because of anamorphic distortion, a normal characteristic of gratings used in the off-Littrow mode. The corrected images shown here are stretched in the dispersion direction by factors of 1.0776 (G750M/6581 Å) and 1.1223 (G430M/4961 Å) to achieve 0.″0507 × 0.″0507 pixels. Wavelength scales are shown in the LMC rest frame.

SONNEBORN et al. (see 492, L140)

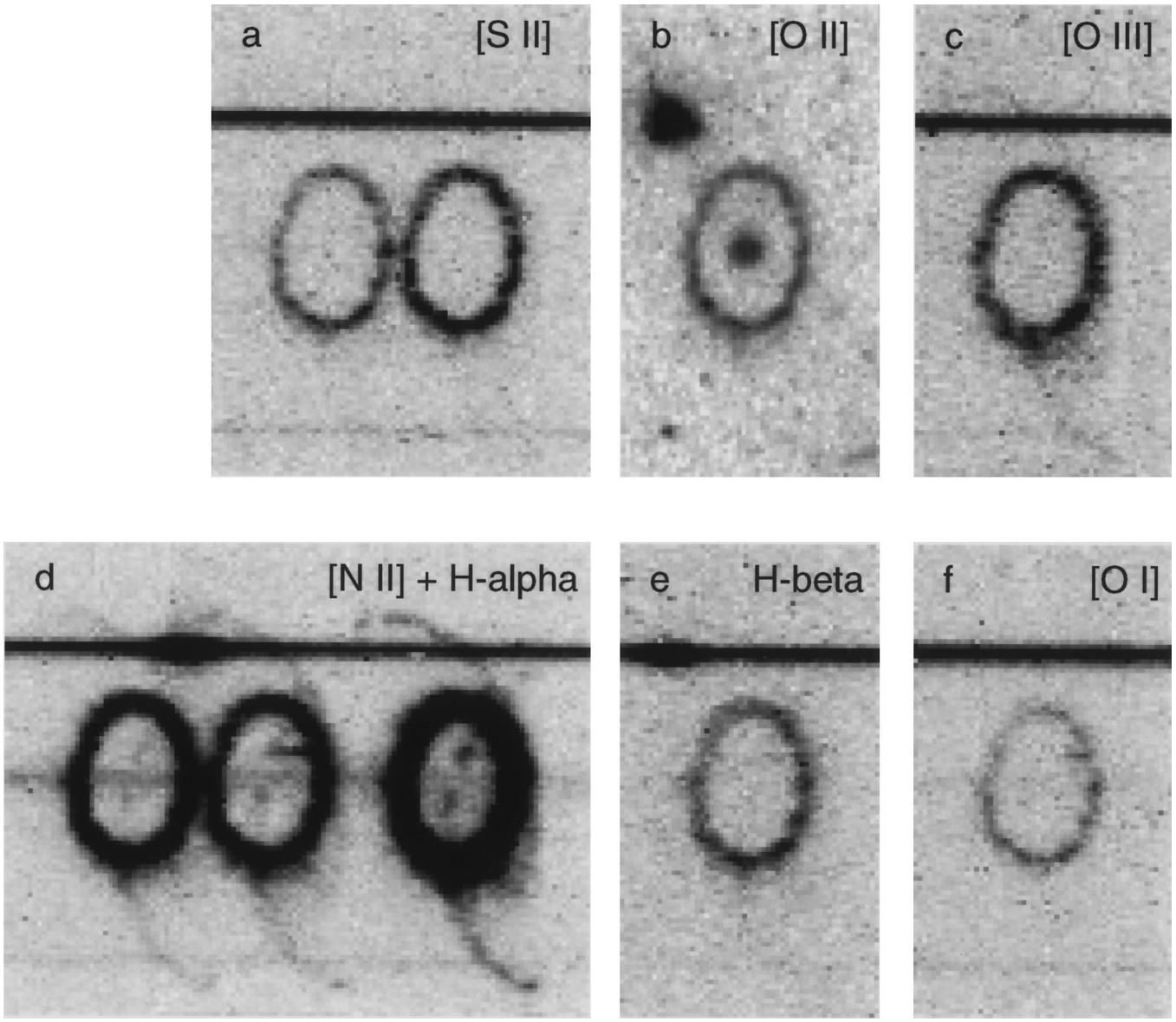

FIG. 6.—STIS images of the SN 1987A inner CS ring. (*a*) [S II] λ6716 and λ6731. (*b*) [O II] λ3727. (*c*) [O III] λ5007. (*d*) [N II] λ6548, Hα, [N II] λ6583. (*e*) Hβ. (*f*) [O I] λ6300. Images (*a*), (*c*), (*d*), (*e*), and (*f*) are subarrays of the images shown in Fig. 3. The wavelength increases from left to right. The [O II] direct image (*b*) was taken with the F28X50OII filter; the SN 1987A debris and star 3 are visible (cf. Fig. 1). The pixel size of these images is 0.″05 × 0.″05.

SONNEBORN et al. (see 492, L141)

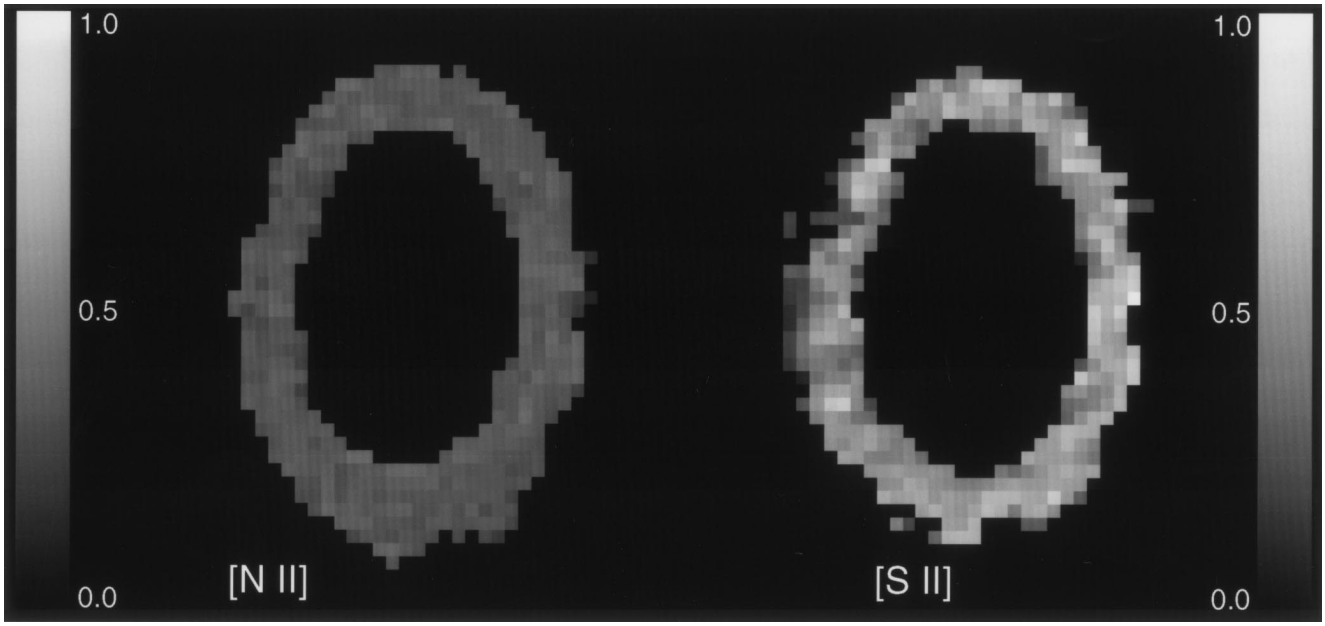

FIG. 8.—Brightness ratios [S II] λ6716/λ6731 (*right*) and [N II] λ6548/λ6583 (*left*) for the SN 1987A inner ring from the G750M exposure. For the [N II] ratio, only points with errors less than 0.25 are included, a total of 373 points.

SONNEBORN et al. (see 492, L142)